Oscillator Array Models for Associative Memory and Pattern Recognition

Paolo Maffezzoni, *Senior Member, IEEE*, Bichoy Bahr, *Student Member, IEEE*, Zheng Zhang, *Student Member, IEEE*, and Luca Daniel, *Member, IEEE*

I. Introduction

Driven by the continuous progress in CMOS fabrication technology, digital computers based on Von-Neumann machine have reached unprecedented computational capability. In spite of that, it is well recognized that there are still classes of computational problems, such as data classifica-tion and recognition, where conventional digital computers perform very poorly compared to the elementary skill of human intelligence. For these applications, it is expected that unconventional brain-inspired neurocomputing characterized by a massive parallelism could lead to significant advances [1]. Arrays of weakly coupled oscillators represent a promising approach to unconventional computation. It has been proved that oscillator arrays can implement computational tasks such as pattern recognition and associative memory by exploiting their natural attitude to synchronization [2]–[4]. In these oscillator arrays, data information is commonly encoded in the relative phase differences achieved at synchronization, which makes computation robust against intrinsic noise of circuit implementation.

However, while the associative memory capability has been proved in principle using ideal oscillator models and couplings, the actual implementation with physical devices still presents many unsolved challenging issues. A first issue is related to finding oscillatory devices and coupling ways that allows a precise control of the array response in terms of relative phase differences. Intuition suggests that proper coupling methods are those that produce phase modulation while minimally affecting oscillating amplitudes.

A second crucial issue consists in developing a robust design methodology. An oscillator array contains a huge number of free parameters that determine its dynamics and synchronization properties. Furthermore, the analysis of the phase response of medium/large oscillator arrays via transistor-level simulation is totally unfeasible due to the prohibitively long simulation times it would take. Behavioral models of oscillators and couplings are thus mandatory to enable oscillator arrays design and associative-memory function verification.

In this paper, we describe an efficient simulation and design approach for arrays of resonant oscillators coupled through transconductance elements. The methodology is developed in the paper by referring to a LC tank oscillatory device but it can be applied to other resonant nano-oscillators fabricated in emerging technologies, such as MEMS resonant body transistor [5]. Extensions to non-resonant oscillators [6]-[7] are also possible in principle and will be the subject of future investigations.

First, we report detailed circuit-level simulations for the case of an elementary array formed by two coupled oscillators. These simulations provide fundamental evidences about the oscillator responses and the shape of the coupling currents. Second, we exploit the above gained insights to provide a realistic phase-domain macromodel of the oscillator array. Such a macromodel is a generalization of previously presented ones [8]-[11] in that it can incorporate the relevant array nonidealities, such as the nonlinear nature of coupling, the variability of oscillating frequency and the unavoidable intrinsic noise. By means of a series of simplifications, we show how the proposed model can be linked to the theory of oscillating computing available in the literature [1], [2], [12]. This theory is in fact essential to highlight the associative memory capability of oscillator arrays. Finally, efficient simulations are carried out with the nonlinear phase-domain model to check the actual associative-memory performance for a bench-mark case study. It is investigated how nonidealities and coupling strength affect the associative memory capability. The aforementioned issues are organized in the paper as follows: Sec. II analyses the elementary array with two coupled resonant oscillators. In Sec. III, we provide the detailed phase-domain model of the oscillator array and we link it to the theory of oscillator neurocomputing. Sec. IV, describes the

P. Maffezzoni is with the Politecnico di Milano, Milan, Italy. E-mail: pmaffezz@elet.polimi.it.
B. Bahr, Z. Zhang and L. Daniel are with the Massachusetts Institute of Technology (MIT), Cambridge, MA, USA. E-mail: (bichoy,z zhang,luca)@mit.edu.

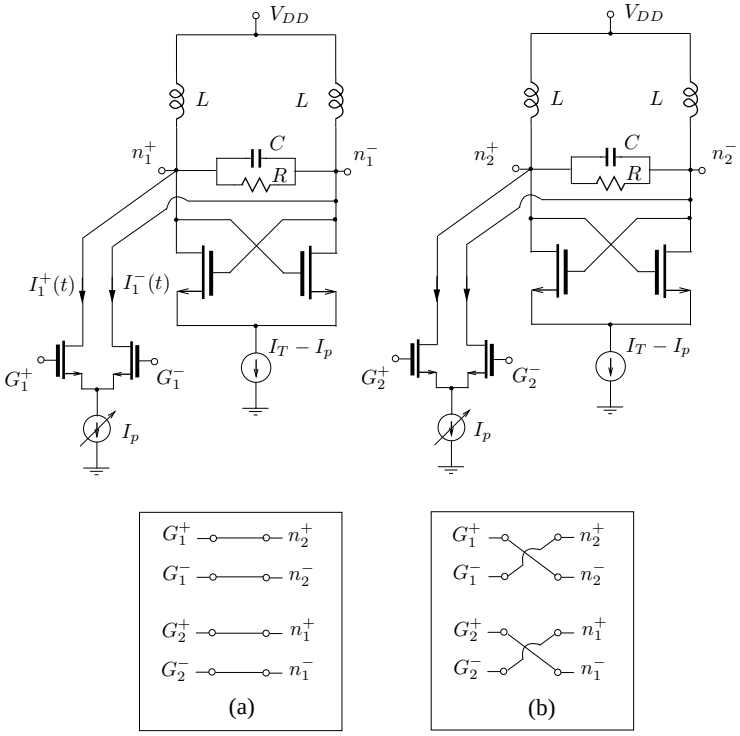

Fig. 1. Coupled LC oscillators. We consider the two different coupling ways (a) and (b) shown in the boxes.

TABLE I

PARAMETERS OF THE LC OSCILLATOR

Parameter	Value
V_{DD}	2.5 V
I_T	460 μA
C	0.3 pF
L	40 nH
R	11 kΩ
(W/L)	30

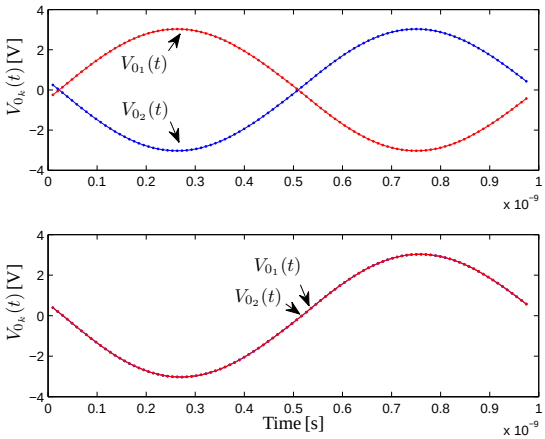

Fig. 2. Array outputs in case a) and b).

associative memory procedure for pattern recognition. Finally, in Sec. V we illustrate numerical experiments for a benchmark case study.

II. TWO COUPLED RESONANT OSCILLATORS

In this section, we analyze in details the elementary array shown in Fig. 1 composed of two LC oscillators. The two oscillators have the identical nominal parameters reported in Table-I. When working in free-running mode (i.e., with no couplings) the two devices oscillate at the same frequency of 1.0261 GHz and their output voltages $V_{0_1}(t) = V_{0_2}(t)$ (measured across the two LC tanks) are purely sinusoidal waveforms with peak values of 3.1 V. The oscillators are coupled through differential pair transistors whose transconductance is controlled by a programmable current source I_p. Such current sources are usually found in current-steering digital to analog converters [13].

For this elementary array, we perform a series of detailed electrical simulations considering the two different ways a) and b) of inserting the coupling transistors shown in the boxes in Fig. 1. We repeat simulations for several values of the polarization current I_p. Fig. 2 shows the output voltages of the coupled oscillators in the two cases a) and b) and for $I_p = 20\,\mu$A. In Case a), the two oscillators synchronize in *anti-phase* while in Case b) they synchronize *in-phase*. In both cases, the output voltages $V_{0_1}(t)$ and $V_{0_2}(t)$ remain sinusoidal with the same peak value as in the free-running mode. This indicates a first evidence about the coupling circuit in Fig. 1: it produces phase modulation of the oscillator responses without affecting their amplitude.

Fig. 3 shows the differential current [1]

$$I_{D_1}(t) = (I_1^+(t) - I_1^-(t))/2 \tag{1}$$

which is injected by oscillator 2 into oscillator 1 for two different polarization currents $I_p = 20\,\mu$A and $I_p = 30\,\mu$A of the coupling transistors. The differential pair works as a harsh comparator and thus its output differential current $I_{D_1}(t)$ is well approximated by the sign function of its input voltage [14], i.e.

$$I_{D_1}(t) \approx g_{12} \cdot \text{sign}(V_{0_2}(t)). \tag{2}$$

In addition, we see that by selecting the polarization current I_p we are able to control the amplitude g_{12} of the injected current, i.e. we can modulate the strength of coupling. The evidences above lead us to the schematic model plotted in Fig. 4 where mutual coupling is achieved through transconductance elements. The module of transconductance parameters $g_{12} = g_{21}$ [2] determines the coupling strength while their sign depends on the way the gates of coupling transistors are connected to the output nodes: Case a) in Fig. 1 corresponds to a positive $g_{12} = g_{21}$ parameter (which leads to anti-phase synchronization) whereas Case b) corresponds to a negative $g_{12} = g_{21}$ parameter (which leads to in-phase synchronization).

[1]Common mode current $I_C(t) = (I_1^+(t) + I_1^+(t))/2$, which is almost constant, is filter out by the LC tank and thus can be neglected.

[2]For reasons that will be clear later, we consider symmetric couplings.

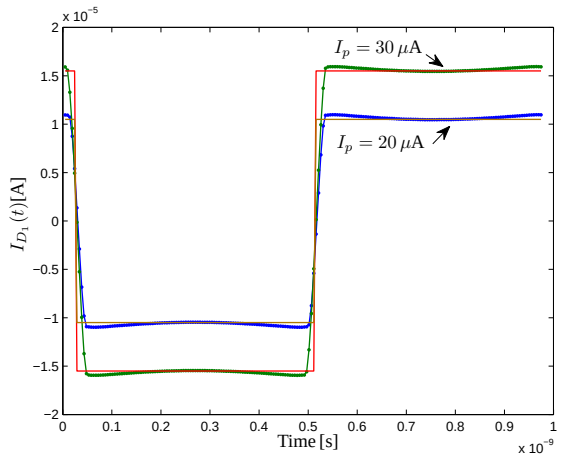

Fig. 3. Injected differential currents. (Dotted line) simulated, (Continuous line) approximated by $g_{12} \cdot \text{sign}(V_{0_2}(t))$.

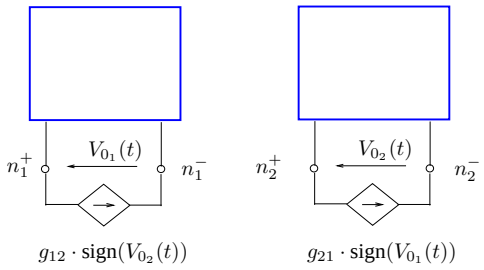

Fig. 4. Schematic model of coupling.

III. Array of Mutually Coupled Oscillators

We pass now to study an array with N LC oscillators coupled through differential pair transistors. Each oscillator of index n can be coupled to any other of index j with a transconductance g_{nj}, as schematically shown in Fig. 5. Couplings are symmetric, i.e. $g_{nj} = g_{jn}$.

First, we present a nonlinear phase-domain of the array that is able to incorporate the relevant nondidealities of the system. Such a detailed model allows performing realistic numerical simulations of the synchronization response in relatively short times. Second, we derive a simplified model of the array. This simplified model is needed to link our model to the theoretical results available in the literature about oscillator neurocomputing.

A. Nonlinear Phase-Domain Model for Numerical Simulations

We denote $V_n(t) = V_M \cos(\omega_n t)$ the output voltage of the nth oscillator when working in free-running mode, where ω_n is its angular frequency. Oscillators are nominally identical and are designed to oscillate at the same nominal angular frequency ω_0. In practical implementations, however, small mismatches among devices may introduce tiny variations of the oscillating frequencies $\omega_n \approx \omega_0$.

When the oscillators are connected via coupling transistors, the mutually injected differential currents produce phase

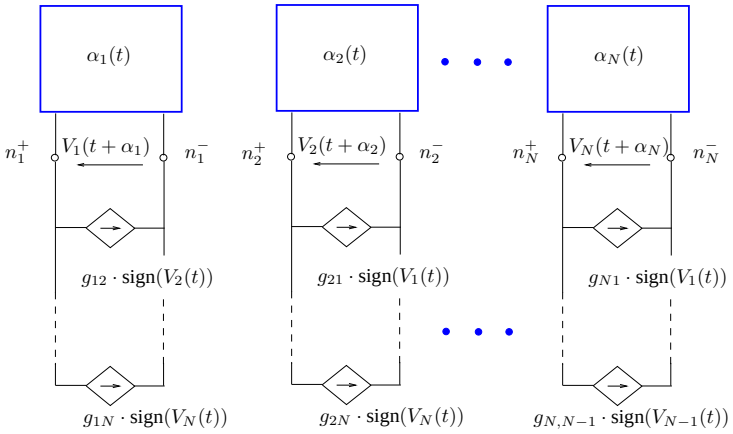

Fig. 5. Array with N coupled oscillators.

modulation of their responses. As a consequence, the output voltage of the nth oscillator can be written as

$$V_n(t + \alpha_n(t)) = V_M \cos(\omega_n t + \omega_n \alpha_n(t)) = V_M \cos(\theta_n(t)) \tag{3}$$

where $\alpha_n(t)$ is the time shift due to phase modulation, $\theta_n(t) = \omega_n t + \omega_n \alpha_n(t)$ is the total phase and $\phi_n(t) = \omega_n \alpha_n(t)$ represents the excess phase.

The phase-domain model of the array is thus given by the following set of equations:

$$\dot{\alpha}_n(t) = \Gamma_n(t + \alpha_n(t)) I_{D_n}(t) \tag{4a}$$

$$I_{D_n}(t) = \sum_{j=1}^{N} g_{nj} \,\text{sign}[V_j(t + \alpha_j(t))], \tag{4b}$$

for $n = 1, \cdots, N$. The function $\Gamma_n(t)$ in (4a) is a T_n-periodic time function that describes the periodically-varying phase sensitivity to the injected current $I_{D_n}(t)$ [15]. This function can be calculated through simulations of the free-running oscillator with specialized numerical techniques [16], [17] as well as with commercially available CAD tools [18]. Eq. (4b) gives the total differential current $I_{D_n}(t)$ injected into oscillator of index n.

The condition for mutual synchronization of the array is that, asymptotically for $t \to \infty$, the total phase difference between any couple of oscillators of index n and j tends to a constant value θ_{nj} [19], i.e.

$$\lim_{t \to \infty} \theta_n(t) - \theta_j(t) = \theta_{nj}. \tag{5}$$

At synchronization all devices oscillate with a common angular frequency ω_c. For the nth oscillator, it is thus possible to define the angular variable $\psi_n(t)$ that measures the deviation of its total phase from the synchronization common one $\omega_c t$, i.e.

$$\psi_n(t) = \theta_n(t) - \omega_c t = \omega_n t + \omega_n \alpha_n(t) - \omega_c t = \phi_n(t) + \Delta\omega_n^c \, t \tag{6}$$

where $\Delta\omega_n^c = \omega_n - \omega_c$ is the frequency detuning from ω_c. Note that in the ideal case of identical oscillating frequencies $\omega_n = \omega_0 = \omega_c$, we have that $\Delta\omega_n^c = 0$ and thus $\psi_n(t) = \phi_n(t)$.

We conclude that, for a given matrix $G = \{g_{nj}\} \in \mathbb{R}^{N\times N}$ of transconductance values, the phase-domain model (4) allows us to simulate, in a numerically efficient way, the time evolution of the total phase variables $\theta_n(t)$ and to check whether synchronization condition (5) is verified or not. In these simulations it is possible to include the variability of oscillating frequencies ω_n. The model can be further enhanced by including the effects of internal noise sources. To this aim, (4a) is modified as follows

$$\dot{\alpha}_n(t) = \Gamma_n(t + \alpha_n(t))I_{D_n}(t) + \eta^n_{eq}(t), \tag{7}$$

where $\eta^n_{eq}(t) = \eta^W_{eq}(t) + \eta^F_{eq}(t)$ is a macro noise source that reproduces the effects of white and flicker noise within the nth oscillator [20], [21].

B. Simplified model for Theoretical Investigation

In this subsection, instead, we move in the direction to simplify the model (4) so as to highlight its intrinsic associative memory capability. First, we exploit the fact that the sensitivity function $\Gamma(t)$ of harmonic oscillators is well approximated by a sinusoid waveform delayed by $\pi/2$ with respect to the output response [11], [22], i.e.

$$\Gamma_n(t) = \Gamma_M \cos(\omega_n t - \pi/2), \qquad \text{for any } n. \tag{8}$$

Second, we use averaging [23], [24]. The average shape of the function $\alpha_n(t)$ obtained by integrating in time (4) can be approximated by using the simplification

$$\text{sign}(V_M \cos(x)) \approx \cos(x) \tag{9}$$

within (4b). Thus, we substitute (4b) with the simplification (9) into (4a) and use (3) and (8), obtaining

$$\begin{aligned} \dot{\alpha}_n(t) \quad &= \quad \Gamma_M \cos(\omega_n t + \omega_n \alpha_n(t) - \pi/2) \\ &\quad \cdot \sum_{j=1}^{N} g_{nj} \cos(\omega_j t + \omega_j \alpha_j(t)). \end{aligned} \tag{10}$$

Keeping only the slowly varying terms that result from the cosine products in (10), we get the averaged equations for the total phase variables

$$\dot{\theta}_n(t) = \omega_n + B \cdot \sum_{j=1}^{N} s_{nj} \sin(\theta_j(t) - \theta_n(t)), \tag{11}$$

where

$$-\sigma_n \cdot s_{nj} = g_{nj}, \tag{12}$$

and

$$\sigma_n = \frac{2\,B}{\omega_n\,\Gamma_M}. \tag{13}$$

With the notation above, the simplified model (11) looks very similar to the well known Kuramoto model [2], [12] where the parameters s_{nj} are the *connection coefficients* while the parameter B determines the *strength of coupling*. The parameters σ_n defined in (13) give the *scaling factors* that allow us to map the "abstract" connection coefficients s_{nj} of the Kuramoto model into concrete transconductance values g_{nj} of the coupling transistors. It is also interesting to note that the connection coefficients s_{nj} have the opposite sign of the related transconductance coefficients g_{nj}. Thus, a positive s_{nj} coefficient favors in-phase synchronization between oscillators of index n and j while a negative s_{nj} favors anti-phase synchronization.

Eq. (11) can then be recast in terms of total phase deviations defined in (6) as follows

$$\dot{\psi}_n(t) = \Delta\omega^c_n + B \cdot \sum_{j=1}^{N} s_{nj} \sin(\psi_j(t) - \psi_n(t)). \tag{14}$$

By extending the approach in [2], it is possible to prove the following result: if the symmetry property $s_{nj} = s_{jn}$ holds, the phase model (14) is the gradient of the function

$$U(\psi_1, \psi_2, \ldots, \psi_N) = -\frac{B}{2} \sum_n \sum_j s_{nj} \cos(\psi_j - \psi_n) - \Delta\omega^c_n\,\psi_n, \tag{15}$$

i.e.,

$$\dot{\psi}_n(t) = -\frac{\partial U}{\partial \psi_n}. \tag{16}$$

As a consequence

$$\frac{dU}{dt} = \sum_{n=1}^{N} \frac{\partial U}{\partial \psi_n}\dot{\psi}_n = -\sum_{n=1}^{N} |\dot{\psi}_n|^2 \leq 0. \tag{17}$$

This means that, if oscillators are mutually synchronized, the vector of their phase deviations $(\psi_1(t), \psi_2(t), \psi_N(t))$, always converges to an equilibrium point where $\dfrac{\partial U}{\partial \psi_n} = 0$ and $\dot{\psi}_1(t) = \dot{\psi}_2(t) = \dot{\psi}_N(t) = 0$ which is a local minimum of the function U.

Depending on the connection coefficients s_{nj}, the function U can have many of such minima with any of them representing a stored/known pattern. Starting from a given initial phase deviation vectors, which represents a new pattern to be recognized, the array will evolve towards the stored pattern which is closest according to its internal "dynamic metric"; the array will thus work as an associative memory. It is worth underlining that the theory developed in this subsection holds provided that oscillator array keeps synchronized and this can be verified via numerical simulations of (4).

IV. Associative Memory for Pattern Recognition

A. Information Encoding

Information can be encoded into the array by taking one of the oscillators and its total phase deviation as a reference, denoted $\theta_1(t)$, and then defining the relative phase differences

$$\Delta\theta_n(t) = \theta_n(t) - \theta_1(t), \tag{18}$$

where $\Delta\theta_1(t) = 0$ by construction. The constant value that the nth phase difference assumes at synchronization $\Delta\theta_n = \theta_{n,1}$ determines the nth element

$$\xi_n = \cos(\Delta\theta_n), \tag{19}$$

of the output vector

$$\vec{\xi} = \{\xi_1, \xi_2, \ldots, \xi_N\}. \tag{20}$$

The element $\xi_n \in (-1, 1)$ of the output vector can be seen as the gray level (white for $+1$ and black for -1) of a pixel in

a pattern image. Fig. 8 shows, as an example, three different patterns defined over $N = 60$ pixels of a bench-mark case study that we will employ in further simulations.

B. Initialization and Recognition

Suppose that a set of p vectors

$$\vec{\xi}^k = \{\xi_1^k, \xi_2^k, \ldots, \xi_N^k\}, \tag{21}$$

with $k = 1, \ldots, p$ are given and define the p patterns to be memorized in the array. The simplest way to memorize the patterns is to set the connection coefficients with the well known *Hebbian rule* used to train Hopfield neural networks [25]

$$s_{nj} = \frac{1}{p} \sum_{k=1}^{p} \xi_n^k \, \xi_j^k. \tag{22}$$

However, for oscillator arrays a different setting of the connection coefficients is needed to initialize the array according to the pattern to be recognized [2]. If the latter is described by the vector

$$\vec{\xi}^0 = \{\xi_1^0, \xi_2^0, \ldots, \xi_N^0\}, \tag{23}$$

then, during initialization, the connection coefficients are set to the values

$$s_{nj}^0 = \xi_n^0 \, \xi_j^0. \tag{24}$$

From (14) and neglecting detunings $\Delta\omega_n^c$, we see that if $\xi_n^0 \xi_j^0 = 1$ then $\theta_{nj} = 0$ while if $\xi_n^0 \xi_j^0 = -1$ then $\theta_{nj} = \pi$. Thus, during initialization, the array dynamics will converge to the correct equilibrium phase differences $\Delta^0\theta_n$ that substituted in (19) give the pattern-to-be-recognized vector $\vec{\xi}^0$ [2].

In conclusion, the associative-memory operation consists in a two-step procedure:

- *Initialization*: The connection coefficients s_{nj} and the corresponding coupling coefficients g_{nj} are first initialized to the pattern to be recognized according to (24). The array is then allowed to achieve synchronization with this coupling.
  In simulations, this corresponds to integrating in time the phase model (4), with the coefficients (24), while starting from random initial time shifts. Simulation is carried out over a time interval T_{init} until array synchronization is reached. Then, the time shift values $\alpha_n(T_{init})$ are calculated for $n = 1, \ldots, N$.
- *Recognition*: The connection coefficients s_{nj}, and the related coupling coefficients g_{nj}, are now switched to the setting (22) which includes all the memorized patterns collectively. In this condition, the oscillator array moves towards a new phase deviation vector. At synchronization, phase deviation vector provides the recognized output pattern. In simulations, the Recognition step corresponds to integrating in time the phase model (4), with coefficients (22), starting from the initial phase shifts $\alpha_n(T_{init})$, obtained at the previous step. The waveforms of $\alpha_n(t)$ and those of the total phases $\theta_n(t) = \omega_n t + \omega_n \alpha_n(t)$ are calculated over a sufficiently long time interval allowing the array to achieve synchronization. The final phase differences $\Delta\theta_n(t) = \theta_n(t) - \theta_1(t)$, substituted in (19), supply the recognized output pattern.

We conclude this section, by noting that the connection coefficients defined in (24) and (22) are transformed via (12) in a *fully-interconnected* oscillator array. This implies that each oscillator is connected to all of the other $N - 1$ oscillators. To relax this high-connectivity problem, alternative arrangements have been proposed in the literature that employ time-dependent interconnections [2], [26]. In this paper, we adopt a time-varying *switched-interconnected* arrangement where each oscillator, over a given oscillation cycle, is injected only by a subset of $M << N$ oscillators. Formally, at the rth oscillation cycle the transconductance coefficients in (12) are transformed into

$$g_{nj}^{(r)} = -\sigma_n \cdot s_{nj}, \tag{25}$$

where $n = 1, \ldots, N$ and $L_r \leq j < L_r + M$ with $L_r = r \cdot M$, while σ_n are the scaling factors previously defined in (13). At each oscillation cycle, the subset of transconductance couplings is shifted over a new block of M oscillator outputs so as to iteratively cover all of the N oscillators. This corresponds to incrementing by 1 the index r so that the $N \times M$ transconductances $g_{nj}^{(r)}$ cover the $N \times N$ connection coefficients s_{nj} in N/M oscillating cycles.

V. Numerical Experiments

A. Array of two coupled oscillators

In the first numerical experiment, we simulate the mutual coupling of the elementary array in Fig. 1 with the phase-domain model sketched in Fig. 4 and described by equations (4). The results obtained with the phase-domain model are compared with those obtained with the detailed transistor-level simulations described in Sec. II. In this experiment, the two oscillators are considered identical with the parameters reported in Table-I. The output voltage $V_0(t)$ of the free-running LC oscillator and its sensitivity function $\Gamma(t)$ are shown in Fig. 6. The samples of these waveforms are employed in the phase-domain model (4). We consider the two coupling arrangements previously investigated in Sec. II and corresponding to: Case a) $g_{12} = g_{21} = 10\,\mu$S; Case b) $g_{12} = g_{21} = -10\,\mu$S. Starting from arbitrary initial time shifts $\alpha_1(0)$ and $\alpha_2(0)$, the time shifts waveforms $\alpha_n(t)$ are obtained by integrating the phase model (4), then, the total phases $\theta_n(t) = \omega_0 t + \omega_0 \alpha_n(t)$, for $n = 1, 2$ are deduced. Fig. 7 shows the simulated total phase difference $\theta_2(t) - \theta_1(t)$. In both cases, the total phase difference is bounded meaning that oscillators synchronize. In perfect accordance with the results reported in Sec. II, we have that in Case a), the phase difference tends to π giving anti-phase synchronization while in Case b) the phase difference goes to zero giving in-phase synchronization. In both cases, the output voltages $V_n(t) = V_0(t + \alpha_n(t))$ calculated with the phase-domain model are perfectly superimposed to the waveforms shown in Fig. 2 and computed with transistor-level simulations. Similarly, the coupling currents $I_{D_j}(t) = g_{j,n} \cdot \text{sign}(V_n(t))$ provided by the phase-domain model match with good accuracy the waveforms computed with transistor-level simulations, as shown in Fig. 3.

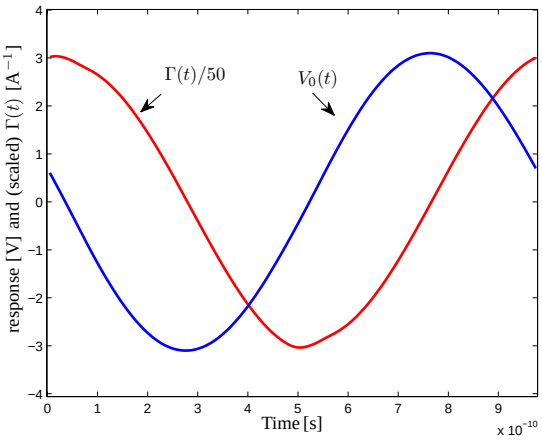

Fig. 6. Free-running response $V_0(t)$ and sensitivity $\Gamma(t)$ of a single LC oscillator for current injection at the tank nodes.

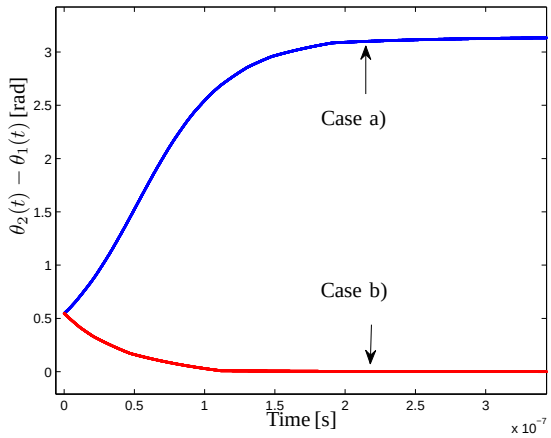

Fig. 7. Phase differences in the elementary array for couplings a) and b).

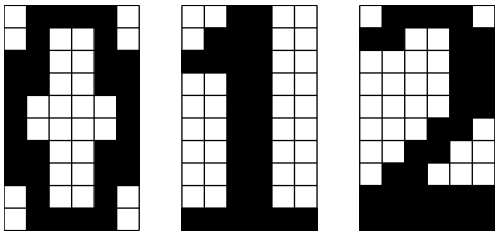

Fig. 8. Patterns memorized in the array.

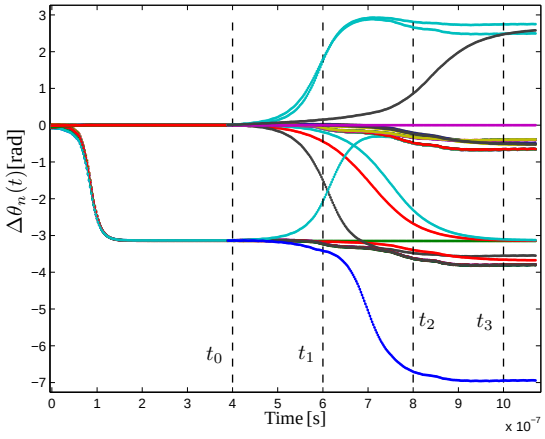

Fig. 9. Phase difference time evolution during the Initialization $0 < t \leq t_0$ and the Recognition simulations $t \geq t_0$. Oscillators synchronize.

This confirms the reliability of the results provided by the phase-domain simulation.

B. Associative memory application

In the second experiment, we consider an array formed with $N = 60$ LC oscillators and implementing the associative memory function described in Sec. IV. The three patterns, described by vectors $\vec{\xi}^k$, to be memorized in the array are shown in Fig. 8.

In these experiments, the oscillators may have different oscillating frequencies $\omega_n \approx \omega_0$. In what follows we consider two different degrees of frequency variability and several coupling strength parameter B values.

In the first case, the frequencies ω_n are randomly generated in a narrow frequency interval of $2\pi \times 100\,\text{kHz}$ centered in ω_0. No internal noise is considered. In this case, a coupling strength of $B = 4 \cdot 10^5$, corresponding to weak coupling currents $I_D(t)$ of the order fractions of μA, is enough to yield array synchronization. Fig. 9 shows the time evolution of the phase differences $\Delta\theta_n(t) = \theta_n(t) - \theta_1(t)$ when the pattern-to-be-recognized shown in Fig. 10 (leftmost pattern at t_0) is loaded in the connection matrix. During the Initialization simulation, i.e. $0 < t \leq t_0 = T_{init}$, the phase differences $\Delta\theta_n(t)$ split into zero or π values and the associated output pattern, computed with (19), just replicates the pattern-to-be-recognized. During the Recognition simulation, i.e. $t \geq t_0$, the phase differences evolve moving towards new constant steady state values close to multiples of π (i.e. array synchronizes). The output patterns computed at the intermediate simulation times t_1, t_2, t_3 and reported in Fig. 10 converge to the correct association. Similar results are obtained for the other patterns, e.g for the distorted pattern "2" shown in Fig. 11. We also verified that the correct pattern recognition occurs for both the fully-interconnected and the switched-interconnected architectures described in Sec. IV-B. In the case of a switched-interconned array, a small ripple appears superimposed to the phase waveforms in Fig. 9 (the ripple is very small and is not shown in the figure). Interestingly, the correct association capability of the array continues to hold if the coupling strength parameter B is increased till about the upper value $B \approx 2 \cdot 10^7$. This upper value corresponds to coupling currents $I_D(t)$ of the order of a few 10μA. For stronger coupling values, mutual synchronization is lost.

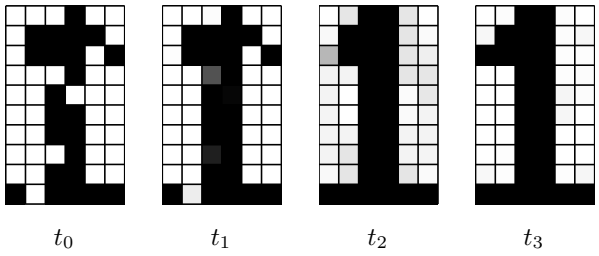

Fig. 10. Sequence of output patterns at different times for a distorted input "1".

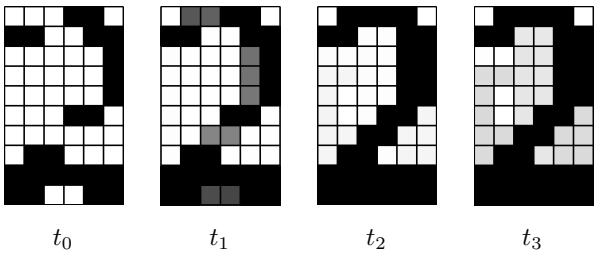

Fig. 11. Sequence of output patterns at different times for a distorted input "2".

Fig. 12 shows that for larger B, during the Recognition simulation, some oscillators desynchronize with the reference and the related phase differences grow with no bounds in time. The corresponding sequence of output patterns shown in Fig. 13 alternates between the correct pattern "1" and the wrong pattern "0".

In the second case, we test the memory association performance for a much greater frequency variability: frequencies ω_n are randomly generated in a frequency interval of $2\pi \times 10\,\text{MHz}$ centered in ω_0. In addition, internal phase noise of each LC oscillator is included in the model as described in (7). Repeated phase-domain simulations show that for large frequency variability mutual synchronization becomes more critical and occurs for a narrower interval of coupling strength values $2 \cdot 10^6 < B < 2 \cdot 10^7$. In the presence of significant frequency variability, in fact, a greater minimum coupling strength is needed to synchronize the oscillator array. Fig. 14 shows the time evolution of the phase differences for the distorted input "1" and for $B = 5 \cdot 10^6$ in a switched-interconnected array with subset block of dimension $M = 5$. Switched interconnection introduces small phase ripples with a period equal to $N/M = 12$ oscillating cycles. After a Recognition simulation time of about 100 oscillation cycles,

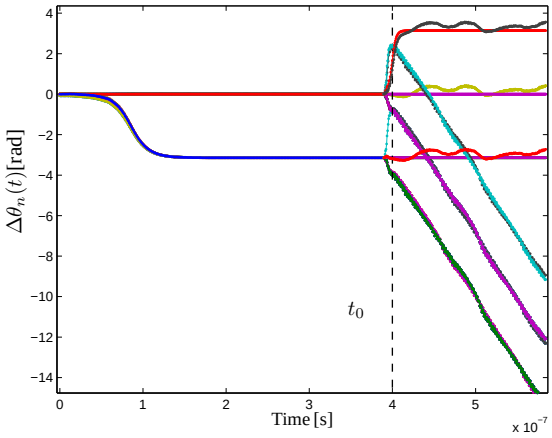

Fig. 12. Phase difference time evolution during the Initialization and Recognition simulations for a too large coupling strength B. Oscillators do not synchronize.

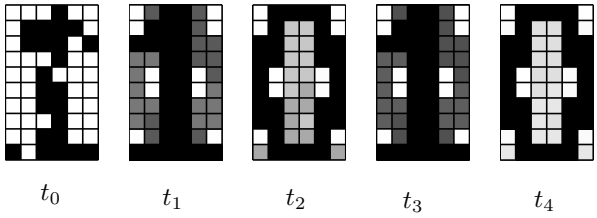

Fig. 13. Sequence of output patterns for a too strong coupling strength and a distorted input "1".

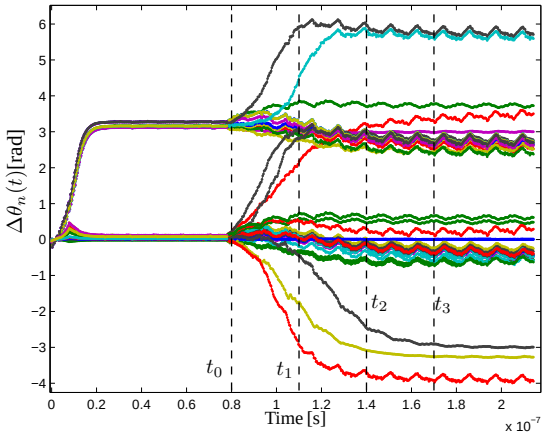

Fig. 14. Phase differences time evolution for large frequency variability computed with a switched-interconnected array.

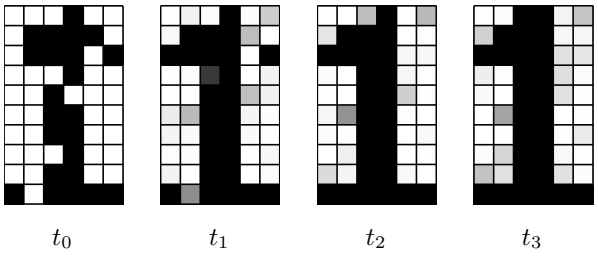

Fig. 15. Sequence of output patterns for a distorted input "1" and large frequency variability.

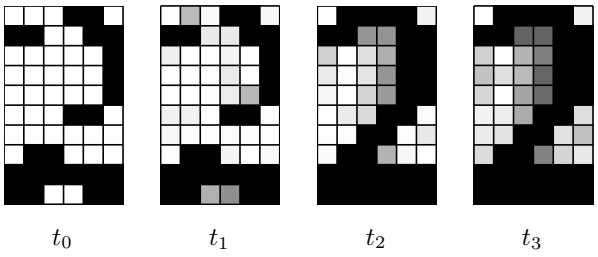

Fig. 16. Sequence of output patterns for a distorted input "2" and large frequency variability.

oscillators synchronize and the phase separations state provides the correct output. However, the almost constant values approached by the phase differences in Fig. 14 are quite spread around multiple of π and this results in the less clean output pattern shown in Fig. 15. A similar result is seen in Fig. 16 for the Recognition of a distorted input "2".

More importantly, we verified that if the Recognition simulation is extended over a longer time interval, e.g. $5,000$ cycles, in some cases, synchronization is eventually lost and a wrong output pattern is associated. A possible justification for such a performance deterioration is that significant frequency detunings $\Delta\omega_n^c$ can produce spurious phase transients, not considered in the simplified analysis in Sec. III. In the long run, such transients may disrupt the associative memory mechanism. Our simulations show that this can be prevented by limiting as much as possible the Recognition time, e.g. to some hundreds oscillation cycles in our example.

VI. Conclusions

In this paper, we have presented a methodological approach to the analysis and design of arrays of resonant oscillators for associative memory applications. A realistic phase-domain model of the oscillator array has been described which is able to incorporate the relevant nonidealities of practical implementations. Relevant nonidealities are the nonlinear nature of coupling, the limited achievable coupling strength as well as the variability of oscillating frequency and phase noise. Simulations have revealed that for very small frequency variability, as it is the case for high Q crystal or MEMs resonators or in the presence of some frequency tuning mechanisms, the correct associative memory behavior holds for a wide range of coupling strength. By contrast, for relatively large frequency variability, e.g. for low Q devices, the associative memory performance results to be strongly affected by the coupling strength. In this case, the proposed phase-domain macromodel provides an invaluable aid to the array design and to the definition of a proper recognition timing.

VII. Acknowledgements

This work was supported in part by the Progetto Roberto Rocca MIT-PoliMI and by the NSF-NEEDs program.

References

[1] F. C. Hoppensteadt and E. M. Izhikevich, *Weakly Connected Neural Networks*, Springer-Verlag, NY, 1997.

[2] F. C. Hoppensteadt and E. M. Izhikevich, Oscillatory neurocomputers with dynamic connectivity, Phys. Rev. Lett., vol. 82, pp. 2983-2986 (1999).

[3] F. Corinto, M. Bonnin, and M. Gilli, "Weakly connected oscillatory network models for associative and dynamic memories", *International Journal of Bifurcation and Chaos*, vol. 17, no. 12, pp. 4365-4379 Dec. 2007.

[4] M. Mirchev, L. Basnarkov, F. Corinto, L. Kocarev, "Cooperative Phenomena in Networks of Oscillators With Non-Identical Interactions and Dynamics," *IEEE Trans. Circuits and Syst. I: Regular Papers*, vol. 61, no. 3, pp. 811-819, Mar. 2014.

[5] R. Marathe, B. Bahr, W. Wang, Z. Mahmood, L. Daniel, and D. Weinstein, "Resonant Body Transistors in IBMs 32 nm SOI CMOS Technology," *Journal of Microelectromechanical Systems*, vol. 23, no. 3, pp. 636-650, June 2014.

[6] S. P. Levitan, Y. Fang, D. H. Dash, T. Shibata, D. E. Nikonov, and G. I. Bourianoff, Non-Boolean associative architectures based on nano-oscillators, *13th International Workshop on Cellular Nanoscale Networks and Their Applications (CNNA)*, 2012, pp. 16.

[7] N. Shukla, et al., "Synchronized charge oscillations in correlated electron systems." *Nature, Scientific reports*, 4, 2014.

[8] D. Harutyunyan, J. Rommes, J. ter Maten, W. Schilders, "Simulation of Mutually Coupled Oscillators Using Nonlinear Phase Macromodels Applications," *IEEE Trans. on Computer-Aided-Design of Integrated Circuits and Systems*, vol. 28, no. 10, pp. 1456-1466, Oct. 2009.

[9] P. Maffezzoni, "Synchronization Analysis of Two Weakly Coupled Oscillators Through a PPV Macromodel," *IEEE Trans. Circuits and Syst. I: Regular Papers*, vol. 57, no. 3, pp. 654-663, Mar. 2010.

[10] M. Bonnin, F. Corinto, "Phase Noise and Noise Induced Frequency Shift in Stochastic Nonlinear Oscillators" *IEEE Trans. Circuits and Syst. I: Regular Papers*, vol. 60, no. 8, pp. 2104 - 2115, Aug. 2013.

[11] P. Maffezzoni, B. Bahr, Z. Zhang, and L. Daniel, "Analysis and Design of Weakly Coupled Oscillator Arrays Based on Phase-Domain Macromodels," *IEEE Trans. Computer-Aided-Design of Integrated Circuits and Systems*, vol. 34, no. 1, pp. 77-85, Jan. 2015.

[12] J. A. Acebrn, L. L. Bonilla, C. J. P. Vicente, F. Ritort, R. Spigler, "The Kuramoto model: A simple paradigm for synchronization phenomena", *Rev. Mod. Physics*, vol. 77, pp. 137-185, Jan. 2005.

[13] M. Gustavsson, J. J. Wikner, N. Nianxiong Tan, *CMOS data converter for communications*, Springer International Series in Engineering and Computer Science, vol. 543, 2000.

[14] P. R. Gray, P. Hurst, S. Lewis, and R. G. Meyer, *Analysis and Design of Analog Integrated Circuits*, NY: Wiley, 2001.

[15] F. X. Kaertner, "Analysis of White and $f^{-\alpha}$ Noise in Oscillators," *International Journal of Circuit Theory and Applications*, vol. 18, pp. 485-519, 1990.

[16] A. Demir, A. Mehrotra and J. Roychowdhury, “Phase Noise in Oscillators: A Unifying Theory and Numerical Methods for Characterisation,” *IEEE Trans. Circuits and Syst. I*, vol. 47, no. 5, pp. 655-674, May 2000.
[17] P. Maffezzoni, “Unified Computation of Parameter-Sensitivity and Signal-Injection Sensitivity in Nonlinear Oscillators,” *IEEE Trans. on Computer-Aided Design of Integrated Circuits and Systems*, vol. 27, N. 5, pp. 781-790, May 2008.
[18] S. Levantino, P. Maffezzoni, “Computing the Perturbation Projection Vector of Oscillators via Frequency Domain Analysis,” *IEEE Trans. Computer-Aided-Design of Integrated Circuits and Systems*, vol. 31, no. 10, pp. 1499-1507, Oct. 2012.
[19] A. Pikovsky, M. Rosenblum, J. Kurths, *Synchronization*, Cambridge Univ. Press, UK 2001.
[20] A. Demir, “Computing Timing Jitter From Phase Noise Spectra for Oscillators and Phase-Locked Loops With White and $1/f$ Noise *IEEE Trans. Circuits and Syst. I*, vol. 53, no. 9, pp. 1859-1874, Sep. 2006.
[21] P. Maffezzoni, S. Levantino, “Analysis of VCO Phase Noise in Charge-Pump Phase-Locked Loops,” *IEEE Trans. Circuits and Syst. I: Regular Papers*, vol. 59, no. 10, pp. 2165-2175, Oct. 2012.
[22] A. Hajimiri , T. H. Lee, “A General Theory of Phase Noise in Electrical Oscillator,” *IEEE Journal of Solid-state Circuits*, vol. 33, no. 2, pp. 179-194, Feb. 1998.
[23] P. Vanassche, G. Gielen, W. Sansen, “On the difference between two widely publicized methods for analyzing oscillator phase behavior,” *Proc. ICCAD 2002*, Nov. 2002, pp. 229-233.
[24] M. I. Freidlin and A. D. Wentzell, *Random Perturbations of Dynamical Systems*, Berlin, Germany: Springer-Verlag, 1984.
[25] D. W. Patterson, *Artificial Neural Networks: Theory and Applications*, Prentice-Hall, New Jersey, 1998.
[26] K. Kostorz, R. W. Holzel, and K. Krischer. “Distributed coupling complexity in a weakly coupled oscillatory network with associative properties,” *New Journal of Physics*, vol. 15, no. 8, pp. 0830100(1-14), Aug. 2013.